Journal of Photochemistry and Photobiology A: Chemistry 224 (2011) 38–45

Contents lists available at SciVerse ScienceDirect

Journal of Photochemistry and Photobiology A: Chemistry

journal homepage: www.elsevier.com/locate/jphotochem

Intramolecular charge transfer emission of a new ketocyanine dye: Effects of hydrogen bonding and electrolyte

Tarek A. Fayed*, Mohammed A. El-morsi, Marwa N. El-Nahass

Department of Chemistry, Faculty of Science, Tanta University, 31527 Tanta, Egypt

ARTICLE INFO

Article history:
Received 6 April 2011
Received in revised form 22 August 2011
Accepted 10 September 2011
Available online 17 September 2011

Keywords:
Ketocyanine
Solvatochromic probe
Semiemperical calculation
Metal ion

ABSTRACT

Photophysical and intramolecular charge transfer characteristics of a new ketocyanine dye namely; 2-[3-(4-dimethylaminophenyl)-allylidene]-tetralone (DMAPT) have been studied in organic solvents having different polarities and hydrogen bond donating ability by using steady-state absorption and emission techniques. Spectral data show that increasing solvent polarity results in a significant solvatochromic shift in the absorption maxima and drastic red shifts in the fluorescence maxima, indicating an intramolecular charge transfer character (ICT) of the excited state, and that the solvent-induced dipole moment change is much greater in the excited state than in the ground state. Semiempirical calculations (PM3 and ZINDO/S) were employed to understand the geometric and electronic structure of DMAPT in both ground and excited state. It reveals twisted intramolecular charge transfer character of the excited state due to photoinduced electron transfer from the dimethyl amino group to the carbonyl oxygen. Also, in order to test the sensing properties and control the intramolecular charge transfer interaction of DMAPT, the complexation behavior of DMAPT in ground and excited states with Li^+, Mg^{2+} and Ca^{2+}, has been studied in acetonitrile solutions. The results indicate ground state complex formation between metal ions and the dye. Values of the equilibrium constants for the interaction of metal ions with DMAPT in the S_1 state have also been estimated.

1. Introduction

Fluorescent probes have been intensively used for many purposes in physics, chemistry, biology, and medicine, since such probes make it possible to solve a number of complicated and important problems [1]. Fluorescent probes containing distinct electron donors and acceptors, most often amino and carbonyl groups have been previously synthesized. Ketocyanine dyes have been used widely as fluorescent probes [2]. The presence of electron-donor (amino) and electron-acceptor (carbonyl) groups in the molecule lead to an increase in charge separation upon electronic excitation, and as a result, the electronic transitions depend strongly on the interaction of the dye molecule with its microenvironment. Spectroscopic and photophysical properties of such dyes have been the subject of intensive investigations in recent years [3–5]. The solvatochromic/fluorosolvatochromic behavior makes such dyes good probes for monitoring micropolarity, hydrogen bonding interactions, and for investigation of microenvironmental characteristics of biological systems [6]. Some ketocyanines are also used as laser dyes and have several industrial applications in photopolymer imaging systems [7]. In addition, these dyes have the ability to chelate alkali and alkaline earth cations, which offers prospects for studying the binding of ions on the surface of biological membranes [8–10]. Recently, the effect of electrolytes on ground- and excited-state properties of ketocyanine dyes has been studied [11]. It was observed that Li^+ ions in aprotic solvents bring about a significant change in the spectral properties. Further, a complex is formed between the cation and the dye molecule in the ground (S_0) and the excited (S_1) states. So, the goal of the present study is to report on the photophysical characteristics, of 2-[3-(4-dimethylamino-phenyl)-allylidene]-tetralone (DMAPT) in different solvents. To give insights into the solvatochromic behavior of DMATP, its ground and excited states ICT interactions have been investigated by both experimental and theoretical methods. Also, in order to test the sensing properties and control the intramolecular charge transfer, the interaction of DMAPT with alkaline earth metals like Li^+, Mg^{2+} and Ca^{2+} in acetonitrile has been reported and the spectroscopic properties for DMAPT–metal complexes have been determined.

2. Experimental details

2.1. Materials and methods

The investigated ketocyanine namely; 2-[3-(4 dimethy laminophenyl)-allylidene]-tetralone (DMAPT) was synthesized

* Corresponding author. Tel.: +20 403120708; fax: +20 403350804.
E-mail address: tfayed2003@yahoo.co.uk (T.A. Fayed).

1010-6030/$ – see front matter © 2011 Elsevier B.V. All rights reserved.
doi:10.1016/j.jphotochem.2011.09.004

by condensation of 4-(dimethylamino)-cinnamaldehyde with α-tetralone in ethanol–water mixture (30%, v/v) containing 6% NaOH under stirring over night [12]. The formed violet product was crystallized from ethanol and characterized by IR, ^{1}H NMR, UV–visible and fluorescence spectral measurements. The used solvents like; methanol (MeOH), methanol-d (MeOD), ethanol (EtOH) n-propanol (PrOH), n-butanol (BuOH), n-pentanol (PenOH), acetonitrile (ACN), N,N-dimethylformamide (DMF), dichloromethane (CH_2Cl_2), chloroform ($CHCl_3$), benzene and n-heptane (Hep) were of spectroscopic grade from Aldrich, except for glycerol (Gly) was from Merck and used as received.

Steady-state absorption and emission spectral measurements were carried out using a Shimadzu UV-3101PC scanning spectrophotometer and a Perkin-Elmer LS 50B spectrofluorometer, respectively. In all experiments, 2×10^{-5} M solutions were used. All measurements were carried out under dim light at room temperature using freshly prepared solutions. For fluorescence spectral measurements, the samples were excited at 430 nm except for Hep solution where the excitation wavelength was 415 nm. For measurement of the fluorescence quantum yield (ϕ_f) diluted solutions were used (optical densities at the excitation wavelength is less than 0.2), and an ethanolic solution of Rhodamine 6G was used as a standard (ϕ_f = 0.95) [13].

Complex formation was studied using 2×10^{-5} M dye concentration while the concentrations of Li^+, Mg^{2+} and Ca^{2+} are varied within the range 0.016–2.7 M.

2.2. Semiempirical quantum calculations

Geometrical optimization along with electronic structure and dipole moment calculations of both the ground and excited state of DMAPT has been performed with the help of ArgusLab 4.0 software (Mark A. Thompson, Planaria Software LLC, Seattle, WA) [14]. Precise geometry optimization was obtained by PM3 Hamiltonian, while electronic structure and dipole moments were calculated by using PM3 and ZINDO/S methods. All calculations were performed using the default parameters.

3. Results and discussion

3.1. Theoretical calculations

The geometrical and electronic structures of DMAPT, in both the ground and excited state, have been elucidated using PM3 semiempirical quantum calculations. The optimized molecular structure is shown in Fig. 1(a). The full optimized geometry of DMAPT reflects incomplete twisting of the single bond between the dimethyl aniline moiety relative to the rest of the molecular skeleton twist angle for C13, C14, C15 and C16 is 39.99° which is much lower than 90°, while the dimethyl amino group is in plane with the phenyl ring. This contributes to stabilization of the separated charges and shows the twisted nature of the intramolecular charge transfer excited state (TICT). Table 1 summarizes the calculated bond orders and charge densities on the molecular skeleton. The bond orders calculated after ground state optimization are consistent with the expected ones and indicate extension of the conjugation over the whole molecular skeleton. Meanwhile, the values calculated for the excited state show an inverted alternation where the bonds characterized by single bond characters in the ground state (such as C1–C2, C12–C13, C14–C15, and C18–N21) acquire double bond characters in the excited state and vice versa for C1–O11, C2–C12 and C13–C14 bonds. However, the incomplete twist can allow for the bond C14–C15 to acquire double bond characters upon excitation. These changes indicate a coupling of the dimethyl aniline group as an electron donor with the carbonyl group as an electron acceptor, via the butadiene bridge. Confirmation for this fact comes from charge density calculations where the charge densities on the dimethyl aniline moiety, butadiene-bridge, carbonyl group and tetralone moiety increases from 0.0233, 0.0512, −0.2149 and −0.0714e, respectively, to 0.1974, 0.2385, −0.4719 and −0.291e upon excitation. The photoinduced charge redistribution over the whole molecular skeleton is well represented by plot of the HOMO and LUMO molecular orbitals as illustrated in Fig. 1(b). Semiempirical calculations using ZINDO/S methods were extended to provide the ground and excited singlet state dipole moments as well as some spectral properties in different solvents, Table 1. The solvents were treated as a continuum dielectric model taking into consideration only the value of the dielectric constant of the solvent [15]. These calculations reveal a great enhancement of the dipole moment of the excited singlet state which is characteristic for TICT transition. Furthermore, it is found that the ground and excited state dipole moments increases slightly as the polarity of the solvent increases indicating the enhanced stability of DMATP in polar solvents. However, the calculations show that the transition dipole and oscillator strength of the HOMO–LUMO transition are insensitive to the solvent polarity, see Table 2.

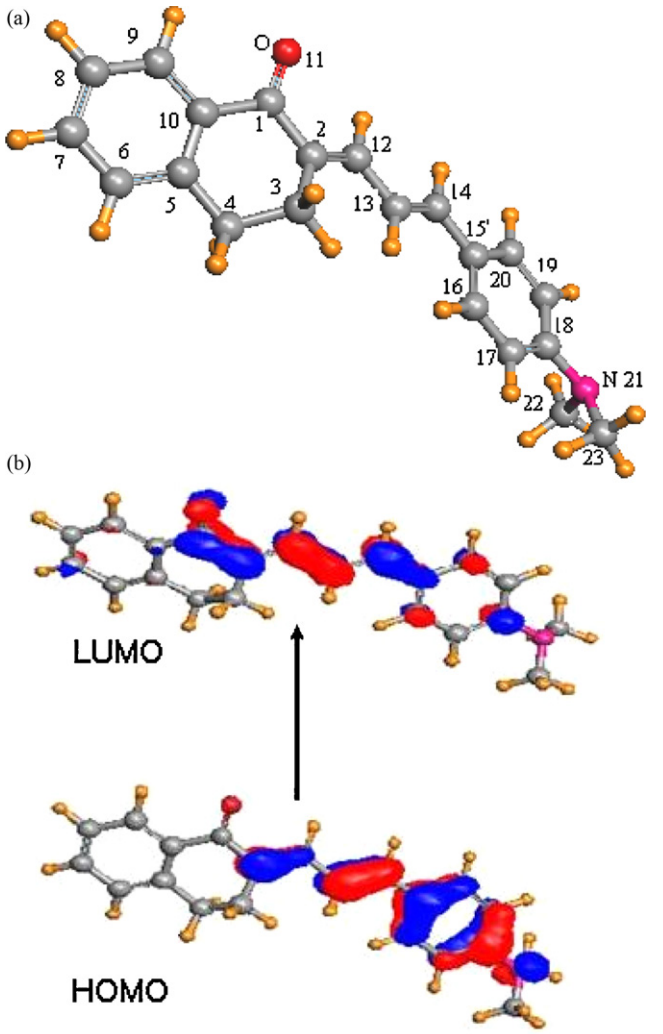

Fig. 1. (a) Optimized geometry of ground state of DMAPT using PM3 calculations. (b) HOMO–LUMO representation.

Due to ICT interactions following excitation, the structure of the excited state DMATP can be presumably represented by a resonance hybrid having contributions from the charge transferred "enol" form, and to a small extent the "keto" form (Scheme 1).

Table 1
Calculated bond orders and charge densities (using PM3 method) on some selected atoms in the ground and first excited singlet states of DMAPT.

Bond	Bond order		Unit	Charge density	
	S_0	S_1		S_0	S_1
C1–C2	1.058	1.125			
C1–O11	1.675	1.473	Butadiene bridge	0.0512	0.2385
C2–C12	1.769	1.419			
C12–C13	1.107	1.28	Carbonyl group	−0.2149	−0.4719
C13–C14	1.787	1.405	Dimethylaniline moiety	0.0233	0.1974
C14–C15	1.083	1.215			
C15–C16	1.385	1.265	Cyclohexanone moiety	−0.1252	−0.3029
C15–C20	1.377	1.272			
C16–C17	1.448	1.5009			
C17–C18	1.405	1.347	Tetralone moiety	−0.0714	−0.291
C18–N21	1.0034	1.017			

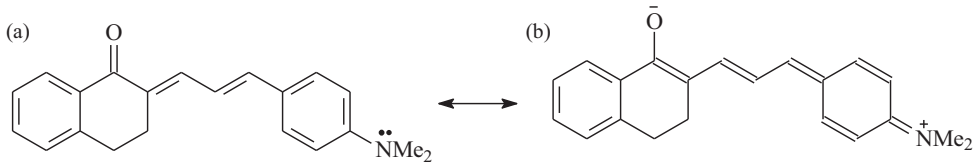

Scheme 1. Resonating structures of DMAPT, "keto" form (a) and the charge-separated "enol" form (b).

The relative weights of the two resonating structures have been found to depend on the solvent polarity [16]. Thus the interaction of the dye molecule with the surrounding polar solvent molecules is greater in the S1 state and the spectra undergo red shifts with increasing the solvent polarity.

3.2. Solvent-induced spectral shifts of DMAPT

In order to explore the nature of solute–solvent interactions, which control the spectral behavior and ICT interactions of DMAPT, it is important to discuss the effects of solvents on its absorption and fluorescence spectra.

Fig. 2 shows the normalized absorption spectra in some solvents. The spectra exhibit a significant broadening (expressed as band width at half maximum, $\Delta\upsilon_{1/2}$, Table 3) as the polarity or acidity (α) of the solvent increases. The intense long-wavelength absorption band (ε_{max} ranges from 2.25 to 2.89×10^4 L mole^{-1} cm^{-1}) undergoes pronounced red-shifts with increasing solvent polarity (ca. 24 nm on going from n-heptane to DMF, Table 3). These features indicate a strongly allowed π–π^* transition with charge transfer characters. Based on the molecular structure and charge density calculations, this absorption band could be attributed to ICT from the dimethylaniline moeity to the carbonyl oxygen in the ground state [17,18].

Fig. 2 displays representative emission spectra of DMAPT in some solvents, while the corresponding fluorescence data are collected in Table 3. In aprotic solvents, the emission spectra are mirror images to the corresponding long-wavelength absorption band and exhibit large red shifts in highly polar solvents. Alcoholic solutions of DMAPT exhibit dual emission as shown in Fig. 3. In fact, the fluorescence excitation spectra recorded at the two respective emission maxima are not identical and do not match exactly with the absorption spectrum, Fig. 4(a). However, the excitation spectrum, monitored at the long-wavelength emission maximum, exhibits a broad band around 452 nm and a shoulder around 406 nm. The excitation maximum at 452 nm corresponds to the long-wavelength absorption band in PrOH, while the shoulder corresponds to the higher energy tail of the absorption band. So, it was concluded that the dual emission in alcohols is due to contribution of two different species present in the ground state. This conclusion was confirmed by recording the excitation spectrum in aprotic solvents like DMF, where only one band which matches the long wavelength absorption band was observed, Fig. 4(b). Based on the foregoing results, these two species are the bare and hydrogen bonded DMAPT molecules with the latter absorbing and emitting at lower energies [19,20].

To further confirm the presence of two ground state species in alcoholic solvents, the effect of excitation energy on the emission

Table 2
Calculated dipole moments (μ, D) and oscillator strength (f) of DMAPT calculated at the ZINDO/S level in different solvents.

Solvent	μ_g	μ_e	μ_{12}	f
Gas phase	6.56(6.5)[a]	12.72	9.33	1.294
Iso-octane	6.7	13.1	9.33	1.289
Benzene	6.8	13.18	9.33	1.288
CH_2Cl_2	7.04	13.59	9.33	1.28
MeOH	7.11	13.71	9.33	1.28
ACN	7.11	13.72	9.33	1.28
H_2O	7.12	13.74	9.33	1.27

[a] Dipole moment calculated using PM3 method.

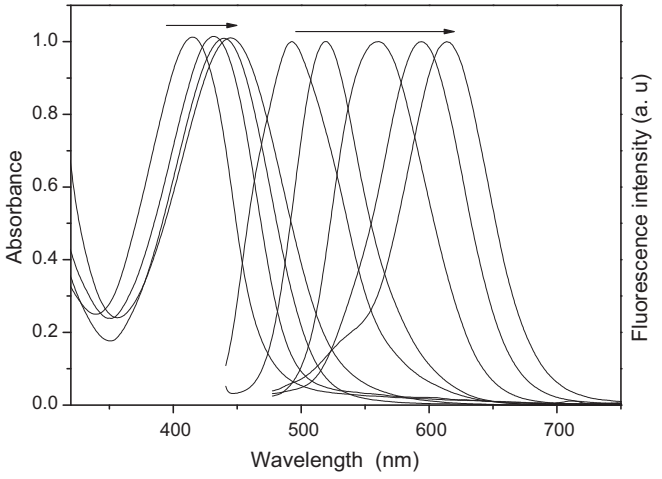

Fig. 2. Normalized absorption (to the left) and emission (to the right) spectra of DMAPT; the solvents in the direction of the arrow are absorption: Hep, benzene, $CHCl_3$ and PenOH, emission: Hep, benzene, $CHCl_3$, ACN and EtOH.

Table 3
Spectral data of DMAPT in various solvents at 25 °C.

Solvent	λ^{a}_{max} (nm)	$\varepsilon \times 10^4$ (l mol^{-1} cm^{-1})	λ^{f}_{max} (nm)	$\Delta\upsilon_{1/2}$ (cm^{-1})	μ_{12}	ϕ_f
Hep	414	2.25	494	4488	6.18	0.133
Benzene	430	2.30	521	4607	6.45	0.284
$CHCl_3$	439	3.55	560	4677	8.16	0.296
CH_2Cl_2	436	2.50	576	5233	7.22	0.32
DMF	438	2.75	591	6006	8.13	0.65
ACN	429	3.0	595	5105	7.75	0.47
n-PenOH	444	2.9	533, 610	5014	7.68	0.39
n-BuOH	447	3.17	532, 614	5105	8.89	0.36
n-PrOH	445	3.05	532, 615	5555	8.306	0.29
EtOH	442	3.11	531, 617	5690	8.46	0.24
MeOD	443	3.361	531, 626	5076	8.31	0.235
MeOH	445	2.891	531, 623	5638	8.14	0.229
Glycerol	466	3.501	620	5437	9.008	0.56
H_2O	437	2.42	597	5986	9.048	0.067

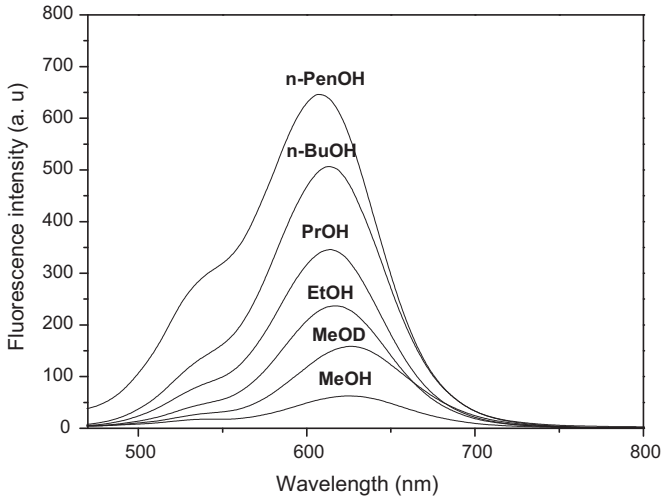

Fig. 3. Fluorescence spectra of DMAPT in aliphatic alcohols.

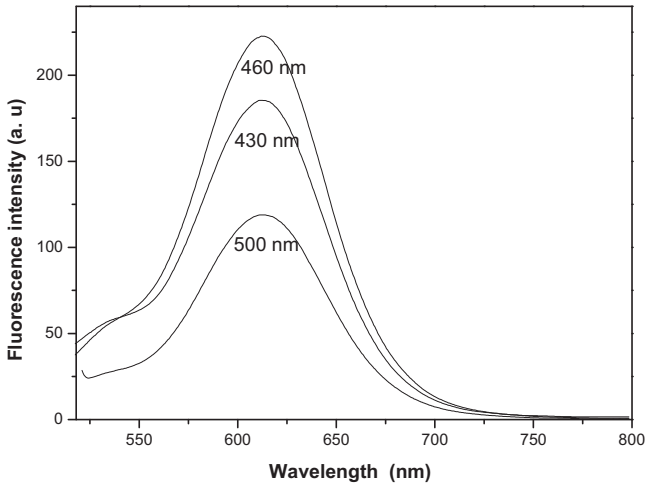

Fig. 5. Fluorescence spectra of DMAPT in *n*-PrOH recorded at different excitation wavelengths.

spectrum in n-PrOH was investigated. Fig. 5 shows that excitation of DMAPT at 430 nm, give rise to two structured emission with a band at 611 nm and shoulder around 526 nm with a remarkable difference in intensities. However, excitation at longer wavelengths leads to enhancement of the emission intensity at 611 nm on the expense of the intensity of the short-wavelength shoulder. Quantitatively, the relative intensity (I_f^{611}/I_f^{526}) increases from 3.7 to 4.26 when the excitation wavelength is changed from 430 to 500 nm, respectively. These changes indicate that excitation at the longer wavelength tail of the absorption band promotes emission from both the free and hydrogen bonded DMAPT molecules.

To get information about the various modes of solvation (e.g. specific or non-specific) which determine the absorption, $E(A)$, and the fluorescence energies, $E(F)$, of DMAPT. $E(A)$ and $E(F)$ were plotted as a function of the Dimorth–Reichardt emperical solvent polarity parameter $E_T(30)$ [21], Fig. 6. The correlations have a

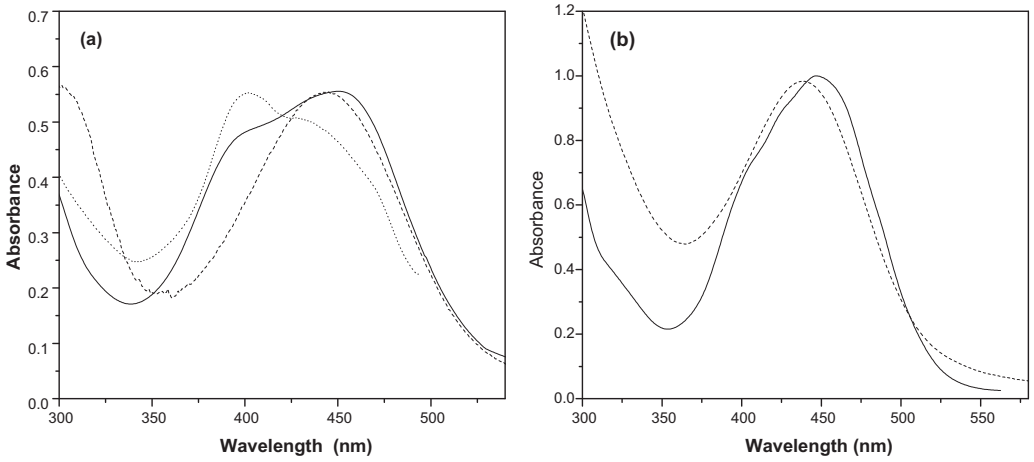

Fig. 4. Excitation spectra of DMAPT in (a) PrOH monitored at 611 nm (—) and 526 nm (. . .) and (b) DMF, monitored at 591 nm. The dashed line is the corresponding absorption spectrum.

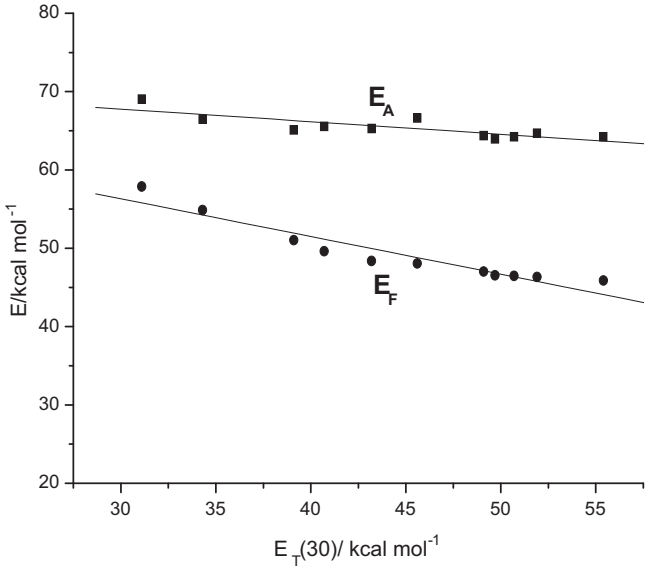

Fig. 6. Dependence of E_A and E_F on the empirical solvent polarity parameter $E_T(30)$ of DMAPT.

negative slope indicating that both absorption and emission maximum is red shifted in highly polar solvents. Also, the enhanced solvent sensitivity of $E(F)$ compared to $E(A)$ is explained in terms of increased solute–solvent interaction in the excited state due to increased dipole moment upon excitation. For alcohols, in addition to dipolar interactions, stronger hydrogen bonding with the solvent molecules is expected in the excited state as a result of increased charge density on the carbonyl oxygen from −0.2149 in the ground state to −0.4719 in the excited state, Section 3.1.

To determine the individual contribution of different modes of solute–solvent interactions that controls the solvent induced spectral shifts a multiparametric approach, known as solvatochromic comparison method (SCM) proposed by Kamlet et al. [22] has been used. This approach separates the dielectric effects of solvents (π^*), hydrogen-bond donor (α) and acceptor (β) abilities of the solvents on the spectral properties. Excluding the data in water, the absorption and fluorescence energies have been analyzed using the SCM according to the following correlations:

$$E(A) = 67.79 - 2.22\alpha - 0.32\beta - 2.3\pi^* \quad r = 0.87 \tag{1}$$

$$E(F) = 60.63 - 6.10\alpha - 3.13\beta - 12.32\pi^* \quad r = 0.94 \tag{2}$$

From Eqs. (1) and (2), it could be observed that the absorption and fluorescence energies are controlled by the cooperative effects of all modes of solvation. The higher coefficients of α, β and π^* in the case of $E(F)$ relative to $E(A)$ reflect the stronger solute–solvent interactions in the excited state and the enhanced hydrogen bonding interaction and higher stabilization of the ICT excited state.

The ground and excited state dipole moments of DMAPT are determined by using the solvent perturbation method [23] based on the absorption and fluorescence shifts in various solvents, according to:

$$\nu_{abs} - \nu_{em} = m_1 f(\varepsilon, n) + const \tag{3}$$

$$\nu_{abs} + \nu_{em} = -m_2[f(\varepsilon, n) + 2g(n)] + const \tag{4}$$

where ν_{abs} and ν_{em} are the absorption and fluorescence band maxima in solvents of varying permittivity (ε) and refractive index (n) [24]. $f(\varepsilon, n) = 2n^2 + 1/n^2 + 2[(\varepsilon - 1/\varepsilon + 2) - (n^2 - 1/n^2 + 2)]$ is the solvent polarity parameter and $g(n) = 3/2[n^4 - 1/(n^2 + 2)^2]$ with

$$m_1 = \frac{2(\mu_e - \mu_g)^2}{hca^3} \quad \text{and} \quad m_2 = \frac{2(\mu_e^2 - \mu_g^2)}{hca^3} \tag{5}$$

Table 4
Experimental data of ground (μ_g, D), excited (μ_e, D) dipole moments, slope and correlation factor of DMAPT by Bilot method.

μ_g (D)	μ_e (D)	$\Delta\mu$ (D)	μ_e/μ_g	m_1 (cm^{-1})	m_2 (cm^{-1})	(r)
4.92	14.11	9.19	2.87	2826.0	5850.2	0.98[a]0.92[b]

[a] Is the slope using the function $f(\varepsilon, n)$.
[b] Is the slope in the case of using $f(\varepsilon, n) + 2g(n)$.

h being Planck's constant and c is the velocity of light in vacuum, μ_g and μ_e are the dipole moments of the ground and excited states. The parameters m_1 and m_2 can be determined from the plots of absorption and fluorescence band shifts ($\nu_{abs} - \nu_{em}$ and $\nu_{abs} + \nu_{em}$) with the solvent polarity parameters according to the above equations. If the ground and excited state dipole moments are parallel, the following expressions are obtained on the basis of above equations [25].

$$\mu_g = \frac{m_2 - m_1}{2}\left[\frac{hca^3}{2m_1}\right]^{1/2} \tag{6}$$

$$\mu_e = \frac{m_2 + m_1}{2}\left[\frac{hca^3}{2m_1}\right]^{1/2} \tag{7}$$

And

$$\mu_e = \frac{m_1 + m_2}{m_2 - m_1}\mu_g; \quad m_2 > m_1 \tag{8}$$

The cavity radius was taken as 40% from the distance between the two farthest atoms in the direction of charge separation within the molecule [26], which was estimated following geometry optimization of DMAPT and comes out to be 6.7 Å. The slopes m_1 and m_2 of the fitted data (according to Eqs. (3) and (4)), as well as the dipole moment values are given in Table 4. The calculated ground and excited state dipole moments are 4.92 and 14.11D, respectively. The values are in good agreement with those obtained theoretically by using PM3 semiemperical calculations (6.5 and 12.72D, in gas phase).

The emission of incomplete TICT excited DMAPT exhibits significant yield (ϕ_f) which is highly sensitive to the solvent polarity and acidity, Table 3. The ϕ_f values decreases steadily as the hydrogen bond donating ability of the solvents increases (ϕ_f value decreases from 0.47 in ACN to 0.23 in MeOH) indicating that hydrogen bonding interactions are controlling strongly the decay of excited DMAPT. As illustrated in Fig. 7, the ϕ_f value increases largely with increasing the solvent polarity (expressed as $E_T(30)$) in aprotic solvents reaching a maximum value in DMF. Further increase in the $E_T(30)$ in protic solvents leads to a decrease in the fluorescence quantum yield. Several mechanisms such as biradicaloid charge transfer, proximity effect (due to coupling between close-lying π–π^* and n–π^* excited states) conformational changes have been proposed to explain the increase of ϕ_f with a suitable enhancement of the intramolecular charge transfer character (negative solvatokinetic effect) [27]. The enhancement of ϕ_f on going from benzene to DMF can be attributed to the strong ICT interaction. The population probability of ICT state depends on the electron donor–acceptor capabilities of the involved partners as well as on the solvent polarity. Polar DMF solvent would stabilize the highly polar ICT state to become below the n–π^* state thus decreasing the probability of population of the non-radiative n–π^* transition. In contrast, the ϕ_f decreases (positive solvatokinetic effect) strongly in highly polar protic solvents like alcohols due to hydrogen-bonding interactions between solvent molecules and the carbonyl group of the fluorophore, which enhance the radiationless internal conversion. To confirm this conclusion, fluorescence quenching of the investigated dye was studied in DMF using some alcohols like MeOH, MeOD, EtOH, n-PrOH, n-BuOH and n-PenOH, as quenchers. The Stern–Volmer constants (K_{SV}) as calculated from the Stern–Volmer

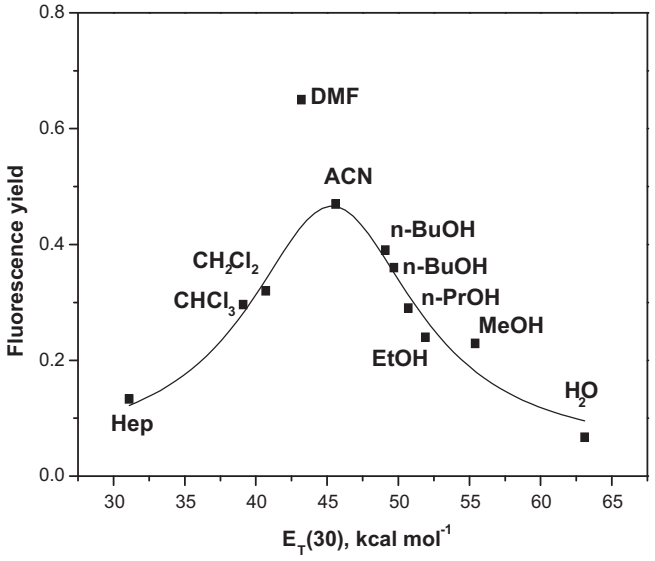

Fig. 7. Variation of the fluorescence yield of DMAPT with the solvent polarity.

plots are 0.447, 0.38, 0.181, 0.17, 0.129 and 0.09 M^{-1} for the previous alcohols, respectively, and increase linearly with the solvent acidity (α) according to the following equation;

$$K_{SV} = -0.649 + 1.079\alpha \quad r = 0.90 \tag{9}$$

This indicates that the quenching mechanism is governed by hydrogen bond formation between the solvent molecules and the excited DMAPT.

The solvent dependence of the fluorescence yield has been also analyzed in terms of a multiple solvent parameters approach collecting the solvent acidity (SA) and basisity (SB), solvent polarity–polarizability (SPP), solvent viscosity (η) and the dipolarity–polarizability (SdP) [28]. Accordingly, the following equation has been obtained ($r = 0.98$):

$$\phi_f = -1.013 - 0.467\text{SA} + 0.162\text{SB} + 1.765\text{SPP} - 0.0158\eta - 0.108\text{SdP}$$

It shows clearly that the solvent dependence of the fluorescence yield is mainly due to solvent acidity and polarity–polarizability effects, while the solvent viscosity has virtually no contribution.

3.3. Spectral features of DMAPT in electrolytes of some alkali metals

In order to test the sensing properties of the present probe to metal ions, the absorption and emission characteristics of diverse cations binded to DMAPT was investigated. Readily detectable cation-induced effects were observed on adding Li^+, Mg^{2+} and Ca^{2+} ions to DMAPT in aprotic dipolar solvent like ACN. Fig. 8 shows the electronic absorption spectra of the interacting DMAPT with Li^+, Mg^{2+} and Ca^{2+} ions in ACN. As shown, on adding Li^+ ions the absorption band maximum of DMAPT appearing at 431 nm decreases and a new lower energy-band appears and it becomes prominent as the concentration of Li^+ increases. Only Li^+ cations have been found to cause pronounced spectral change with an isosbestic point appears at 447 nm. Such results point clearly to the existence of two species in equilibrium. While the lower wavelength band at 431 nm corresponds to the solvated DMAPT, the longer wavelength band (at 458 nm) is presumably due to the Li^+-DMAPT complex. For the interaction of DMAPT with Mg^{2+} and Ca^{2+} ions in ACN, the band shifts only to a small extent with appearance of two isosbestic points at 393, 516 nm for Mg^{2+}, and at 408, 524 nm for Ca^{2+}. All these results confirm the formation of complex between the used metal ions and the investigated dye.

Spectral observations can be rationalized in terms of the existence of the following equilibrium in solution:

$$\text{DMAPT} \ldots \text{S} + \text{M} = \text{DMAPT} \ldots \text{M} + \text{S} \tag{10}$$

Here (DMAPT...S) and (DMAPT...M^{n+}) represent solvated and complexed dye, respectively, the equilibrium constant (K) can be found out by assuming that the observed maximum energy of a spectroscopic transition, $E(A)$ is a mole fraction average of those of the two species, the solvated and complexed form of the dye [29]. Thus, one gets:

$$E(A) = \frac{C_S E_S + C_C E_C}{C_S + C_C} \tag{11}$$

where $E(A)$ is the maximum energy of absorption for a metal ion concentration C_M, E_S and E_C are that for the solvated and the complexed dye, respectively. Eq. (11) can be rearranged to give:

$$E(A) = E_S + E_C K\, C_M - KE(A)C_M \tag{12}$$

Values of E_S, E_C and K that fit Eq. (12) can thus be determined by a linear regression analysis. Values of spectroscopic parameters for the dye metal ion complexes have been summarized in Table 5. The value of E_S, as obtained from the linear regression analysis equals

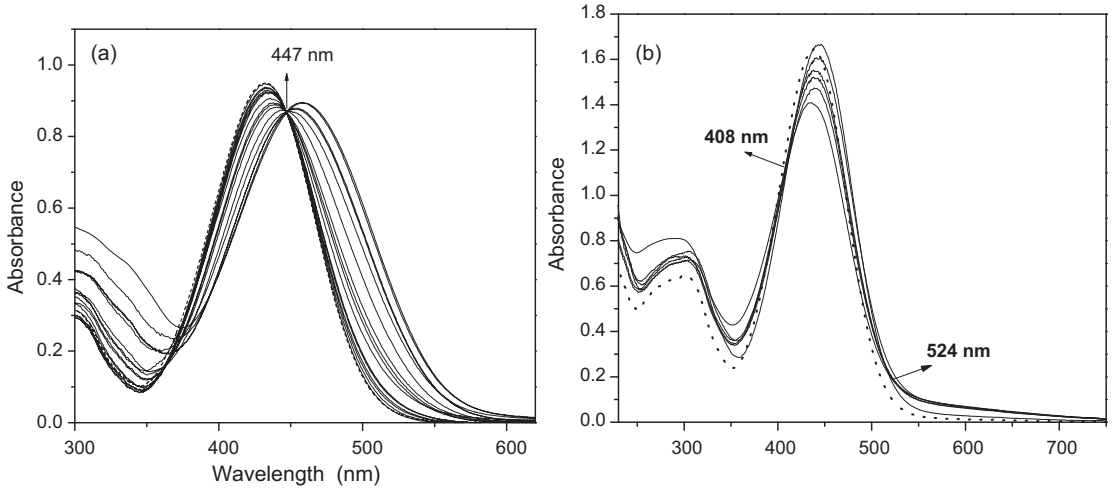

Fig. 8. Absorption spectra of DMAPT containing different concentrations of (a) Li^+ and (b) Ca^{2+} in ACN.

Table 5
Spectroscopic parameters for ground and excited state complexation of DMAPT with various metal ions in ACN.

Metal ion	Ionization potential[a] (eV)	E_S (kcal mole^{-1}	E_C kcal mole^{-1}	K l mole^{-1}	E_{S1} kcal mole^{-1}	E_{C1} kcal mole^{-1}	K_1 l mole^{-1}
Li^+	5.34	64.1	75.18	0.133	48.17	49.3	0.22
Mg^{2+}	7.64	64.48	92.5	0.28	47.73	46.0	1.6
Ca^{2+}	6.11	64.04	57.03	0.82	47.9	45.06	2.26

[a] Values were taken from [33].

64.4 kcal mole^{-1} for DMAPT which agrees with the value measured in ACN (66.3 kcal mole^{-1}).

The fluorescence of DMAPT appears as a broad and structureless band with a maximum around 596 nm in ACN. On addition of Li^+, Mg^{2+} or Ca^{2+} ions, the band maximum is red shifted, Fig. 9. The extent of the red shift is 9, 11 and 20 nm, for Ca^{2+}, Mg^{2+} and Li^+, respectively. The red-shifted band is due to the dye–metal ion complex formation. This was rationalized in view of increased charge density on the carbonyl oxygen in the S_1 state, leading to a stronger dye–metal ion interaction relative to that in the ground state [30]. Supplementary Fig. S1 shows representative plots of the fluorescence energy, $E(F)$, for the complexed dye [E(F)/kcal mole^{-1} = 28590/(λ/nm)] as a function of metal ion concentration.

The observed $E(F)$ can be considered as a mole fraction average of the solvated and the complexed dye, E_{S1} and E_{C1}, respectively. Thus, one gets [31]:

$$E(F) = \frac{C_S E_{S1} + C_C E_{C1}}{C_S + C_C} \quad (13)$$

Eq. (16) can be rearranged to give:

$$E(F) = E_{S1} + E_{C1} K_1 C_M - K_1 E(F) C_M \quad (14)$$

where K_1 is the binding constant for the following process [32]:

$$S \ldots D(S_1 state) + M = M \ldots D(S_1 state) + S$$

Thus, values of E_{S1}, E_{C1} and K_1 that fit Eq. (14) were determined by a linear regression analysis and listed in Table 5. It appears that the value of K_1 is greater than that of K, indicating formation of a relatively stronger complex in the S_1 state.

Alkaline earth metal ions, when present in solution of DMAPT in aprotic solvents, interact with the carbonyl group of the dye, and the relative weight of the "enol" form (Scheme 1) in the ground state as well as in the excited state increases. The interaction of Li^+, Mg^{2+} and Ca^{2+} ions with the S_1 state of DMAPT is expected to be stronger in view of the greater relative weight of the "enol" like structure. This is also reflected by the significantly higher values of the equilibrium constant for complexation involving the S_1 state of DMAPT, Table 5. The nature of the interaction in the weak molecular complex formed between the dye and the metal ion is predominantly electrostatic in nature as reflected from the little variation of E(A) and E(F) with the ionization potential of the metal.

As shown in Fig. 10, the fluorescence of DMAPT was effectively quenched by Li^+, Mg^{2+} and Ca^{2+} ions in ACN, and a new structurless red-shifted emission band is observed at sufficiently higher concentration of the salt, confirming the formation of an emitting complex under these experimental conditions. Representative Stern–Volmer plots are illustrated in Supplementary Fig. S2. The plots show an upward curvature at higher concentrations of metal ions, indicating that static quenching mechanism via ground state complexation is predominant. In such cases, the K_{SV} constants were calculated from the linear part of the plots, where a dynamic process in which quenching is mainly due to collision is taking place. The results can be best fitted by the following equations;

For Li^+ $F_0/F = 1.2347 + 0.44[Q] + 0.57[Q]^2$ $r = 0.994$ (15)

For Mg^{2+} $F_0/F = 0.985 + 1.92[Q] + 69.27[Q]^2$ $r = 0.997$ (16)

For Ca^{2+} $F_0/F = 1.09 + 2.95[Q] + 24.46[Q]^2$ $r = 0.992$ (17)

where F_0 and F are the fluorescence intensities in the absence and presence of the quencher (Li^+, Mg^{2+} and Ca^{2+}), respectively, and Q is the concentration of the metal ions. The results point to the simultaneous existence of static and dynamic quenching. It is interesting to note that the sum of the constants representing ground and excited-state complexation of DMAPT (K and K_1) equals 0.353, 1.88 and 3.08, for Li^+, Mg^{2+} and Ca^{2+}, respectively, which are in close agreement with the coefficient of Q in Eqs. (15)–(17) confirming the dynamic and static quenching modes. The Stern–Volmer constants (K_{SV}) as calculated from the Stern–Volmer plots are 0.45, 8.1 and 6.37 M^{-1} for Li^+, Mg^{2+} and Ca^{2+}, respectively. There was a satisfactory correlation between K_{SV} and the ionization potential of the

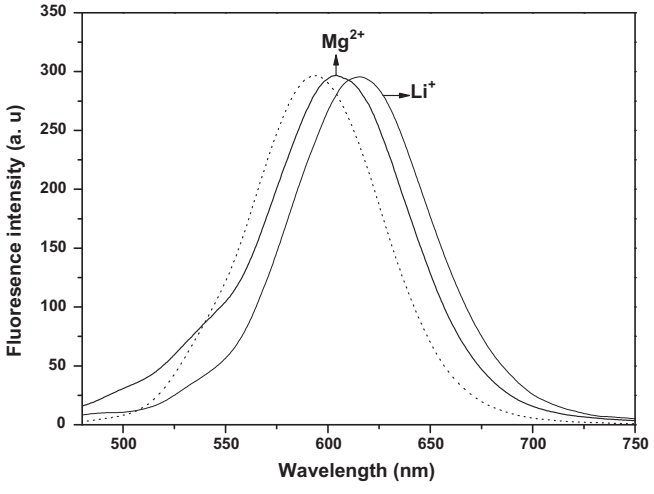

Fig. 9. Fluorescence spectra of DMAPT in ACN solution saturated with Li^+ and Mg^{2+}. The dotted line represents the fluorescence spectra in ACN.

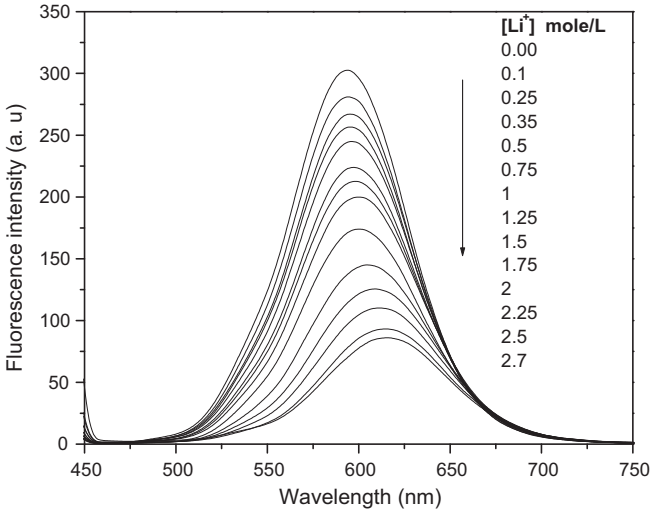

Fig. 10. Changes of fluorescence spectra of DMAPT on adding different concentrations of Li^+ in ACN.

metal [33], Supplementary Fig. S3. The correlation indicates contribution of the electron transfer (from the carbonyl group of the dye to the metal ion) to the quenching mechanism.

4. Conclusion

DMAPT is very sensitive to the solvent polarity and hydrogen bond properties. Spectral data show that increasing solvent polarity results in a significant shift in the absorption and fluorescence maxima, indicating an intramolecular charge transfer (ICT) from the dimethyl amino group to the carbonyl oxygen which is confirmed by theoretical calculations. Electronic absorption and emission spectral characteristics of DMAPT with metal ions such as, Li^+, Mg^{2+} and Ca^{2+} have been studied in acetonitrile solution. Absorption and emission spectra are sensitive to the nature of metal ions. Values of the equilibrium constants for the interaction of metal ions with DMAPT in the S_1 state have also been estimated.

Appendix A. Supplementary data

Supplementary data associated with this article can be found, in the online version, at doi:10.1016/j.jphotochem.2011.09.004.

References

[1] M.A. Thompson, G.K. Schenter, J. Phys. Chem. 99 (1995) 6374–6386.
[2] A.O. Doroshenko, A.V. Grigorovich, E.A. Posokhov, V.G. Pivovarenko, A.P. Demchenko, J. Mol. Eng. 8 (1999) 199–215.
[3] J.R. Lakowicz, Principles of Fluorescence Spectroscopy, 3rd ed., Springer, New York, 2006.
[4] A.O. Doroshenko, A.V. Grigorovich, E.A. Posokhov, V.G. Demchenko, A.D. Sheiko, Russ. Chem. Bull. Int. Ed. 50 (2001) 404–412.
[5] A.O. Doroshenko, V.G. Pivovarenko, J. Photochem. Photobiol. A 156 (2003) 55–64.
[6] A.O. Doroshenko, M.D. Bilokin, V.G. Pivovarenko, J. Photochem. Photobiol. A 163 (2004) 95–102.
[7] V.G. Pivovarenko, A.V. Klueva, A.O. Doroshenko, A.P. Demchenko, Chem. Phys. Lett. 325 (2000) 389–398.
[8] M.V. Barnabas, A. Liu, A.D. Trifanac, V.V. Krougauz, C.T. Chang, J. Phys. Chem. 96 (1992) 212–217.
[9] J.A. Mondal, H.N. Ghosh, T. Mukherjee, D.K. Patil, J. Phys. Chem. A 109 (2005) 6836–6846.
[10] A.O. Doroshenko, A.V. Grigorovich, E.A. Posokhov, V.G. Pivovarenko, A.P. Demchenko, Funct. Mater. 7 (2000) 323–329.
[11] A.O. Doroshenko, A.V. Grigorovich, E.A. Posokhov, V.G. Pivovarenko, A.P. Demchenko, Mol. Eng. 8 (1999) 199–215.
[12] N. Marcotte, S. Fery-Forgues, D. Lavabre, S. Marguet, V.G. Pivovarenko, J. Phys. Chem. A 103 (1999) 3163–3170.
[13] J.K. Basu, M. Shannigrahi, S. Bagchi, Chem. Phys. Lett. 431 (2006) 278–282.
[14] T.A. Fayed, M.K. Awad, Chem. Phys. 303 (2004) 317–326.
[15] H. Du, R.A. Fuh, J. Li, A. Corkan, J.S. Lindsey, J. Photochem. Photobiol. 68 (1998) 141–142.
[16] M.A. Thompson, E.D. Glendening, D. Feller, J. Phys. Chem. 98 (1994) 10465–10476.
[17] N. Kediaa, A. Sarkara, M. Shannigrahib, S. Bagchia, Spectrochim. Acta A Mol. Biomol. Spectrosc. 81 (2011) 79–84.
[18] A. Sarkar, N. Kedia, P. Purkayastha, S. Bagchi, J. Luminescence 131 (2011) 1731–1738.
[19] T.A. Fayed, Chem. Phys. 324 (2006) 631–638.
[20] J.A. Mondal, S. Verma, H.N. Ghosh, D.K. Palit, J. Chem. Sci. 120 (2008) 45–55.
[21] K. Dimroth, C. Reichardt, T. Siepman, F. Bohlman, Liebigs Ann. Chem. 661 (1963) 1–37.
[22] M.J. Kamlet, J.L.M. Abboud, M.H. Abraham, R.W. Taft, J. Org. Chem. 48 (1983) 2877–2887.
[23] L. Bilot, A. Kawasaki, Z. Naturforsch. 17 A (1962) 621–630.
[24] A. Kawasaki, in: J.F. Rabec (Ed.), Progress in Photochemistry and Photophysics, vol. 5, 1, CRC Press, Bocaraton, 1992.
[25] A. Kawasaki, Z. Naturforsch. 57 A (2002) 255–262.
[26] R.M. Hermant, N.A.C. Bakker, T. Scherer, B. Krijinen, J.W. Verboeven, J. Am. Chem. Soc. 112 (1990) 1214–1221.
[27] K. Rurack, M.L. Dekhtyar, J.L. Bricks, U. Resch-Genger, W.J. Rettig, Phys. Chem. A 103 (1999) 9626–9635.
[28] J. Catalan, in: G. Wypych (Ed.), Handbook of Solvents, Chem Tech Publishing, Toronto, 2001, p. 583.
[29] N. Ray, J.K. Basu, M. Shannigrahi, S. Bagchi, Chem. Phys. Lett. 404 (2005) 63–68.
[30] S.K. Sardar, K. Srikanth, S. Bagchi, J. Phys. Chem. A 114 (2010) 10388–10394.
[31] J.K. Basu, M. Shannigrahi, S. Bagchi, J. Phys. Chem. A 110 (2006) 9051–9056.
[32] J.K. Basu, M. Shannigrahi, S. Bagchi, Chem. Phys. Lett. 441 (2007) 336–341.
[33] K.A. Walsh, Handbook of Beryllium Chemistry and Processing, ASM international Publishing, Toronto, 2009.